Biointerphases (2012) 7:17
DOI 10.1007/s13758-011-0017-3

IN FOCUS: NANOMEDICINE - ARTICLE

Dynamic Cellular Uptake of Mixed-Monolayer Protected Nanoparticles

Randy P. Carney · Tamara M. Carney · Marie Mueller · Francesco Stellacci

Received: 17 October 2011 / Accepted: 22 December 2011 / Published online: 9 February 2012

Abstract Nanoparticles (NPs) are gaining increasing attention for potential application in medicine; consequently, studying their interaction with cells is of central importance. We found that both ligand arrangement and composition on gold nanoparticles play a crucial role in their cellular internalization. In our previous investigation, we showed that 66-34OT nanoparticles coated with stripe-like domains of hydrophobic (octanethiol, OT, 34%) and hydrophilic (11-mercaptoundecane sulfonate, MUS, 66%) ligands permeated through the cellular lipid bilayer via passive diffusion, in addition to endo-/pino-cytosis. Here, we show an analysis of NP internalization by DC2.4, 3T3, and HeLa cells at two temperatures and multiple time points. We study four NPs that differ in their surface structures and ligand compositions and report on their cellular internalization by intracellular fluorescence quantification. Using confocal laser scanning microscopy we have found that all three cell types internalize the 66-34OT NPs more than particles coated only with MUS, or particles coated with a very similar coating but lacking any detectable ligand shell structure, or 'striped' particles but with a different composition (34-66OT) at multiple data points.

This article is part of the Topical Collection "In Focus: Nanomedicine".

R. P. Carney, T. M. Carney and M. Mueller contributed equally to the paper.

Electronic supplementary material The online version of this article (doi:10.1007/s13758-011-0017-3) contains supplementary material, which is available to authorized users.

R. P. Carney · T. M. Carney · M. Mueller · F. Stellacci (✉)
Department of Materials Science and Engineering, École Polytechnique Fédérale de Lausanne (EPFL),
1015 Lausanne, Switzerland
e-mail: francesco.stellacci@epfl.ch

1 Introduction

Monolayer-protected nanoparticles (NPs) have generated attention as drug delivery vectors due to their versatility and potential for nanoscale control over surface modification, size, dispersity, core composition, and ionic properties [1–4]. NPs continue to be exploited in a variety of medical processes, including sensing, delivery, and as imaging or contrast agents [5–7]. It has been shown that NP size, shape, and surface properties strongly influence how they interact with cells, including the mechanism of cellular uptake [8]. Here we study NPs consisting of an inorganic gold core coated with a self-assembled monolayer (SAM) of thiolated organic molecules [9]. These surface-bound molecules, or ligands, determine the solubility of the NPs in addition to providing a facile scaffold for additional modification [10, 11], such as the surface conjugation of fluorescent makers, targeting agents or therapeutic agents [12, 13]. However, the study of the supramolecular interactions between the surface ligands and their biological environment is in its infancy, especially for the case of mixed-ligand systems. Currently therapeutic approaches are limited by the poor permeability of the plasma membrane [14]. To enhance the delivery of NP cargo to intracellular targets, a greater understanding of how to manipulate energy-mediated transport processes of cellular barriers must be achieved.

Biological membranes are designed to efficiently protect the internal cellular components from foreign materials. In general, passage across the lipid bilayer follows active or passive transport [15]. Active uptake processes follow

energy-dependent endocytotic or pinocytotic pathways, while passive transport is energy-independent and characteristically reserved for small molecules/particles that diffuse through small protein channels or the lipid bilayer itself [16]. Most delivery vectors are trapped inside endosomal compartments, leading to a weak pharmacokinetic profile [17–19]. Recently, we showed that a particular type of mixed-ligand NP exhibiting order in its structured ligand shell gives rise to passive transport properties through biological membranes [20].

When two immiscible, organic molecules self-assemble onto a flat surface, phase-separation into random domains occurs. We found that when these molecules are self-assembled onto a curved surface (e.g., a NP's core), they spontaneously phase separate into stripe-like domains [21–24]. In order to explore the supramolecular interactions of the ligand shell with the cell membrane, we previously synthesized a series of NPs with identical core size, ligand shell packing density, and zeta potential, only differing in ligand shell morphology [20]. Four types of NPs were synthesized [25]. The first two types of NPs were coated with alternating domains of hydrophobic (octanethiol, OT) and hydrophilic (11-mercaptoundecane sulfonate, MUS) ligands in different percentage ratios of 66-34OT and 34-66OT. The third type of NP, 66-34brOT, has identical hydrophobic and hydrophilic content to the 66-34OT, but is deficient of ordered stripes, synthesized by replacing the OT with a branched version of the molecule, branched-octanethiol (brOT, 2,7-dimethyloctanethiol). The final type, 100MUS, was coated with just a single type of the hydrophilic ligand. The 66-34OT NPs were found to penetrate cell membranes at 37 and 4°C (at which temperature energy-mediated endocytosis is blocked) [20]. The 66-34brOT and 100MUS NPs did not penetrate the cell membrane passively, but were instead endocytosed [20]. Even at 37°C, after blocking endocytosis by treating the cells with endocytotic inhibitors (sodium azide and 2-deoxyglucose), the structured NPs were found to penetrate into the cytosol. In order to rule out membrane poration (which is a known behavior of cationic NPs), the NPs were co-incubated with calcein and no noticeable leakage occurred alongside NP penetration. We concluded that the structural organization of the ligand shell regulated cell-membrane penetration, and that active endocytotic or pinocytotic pathways were not required for the NPs to reach the cytosol of the cells [20]. These results were confirmed by intracellular photothermal heterodyne imaging of the same type of NPs [26]. Additionally recently we have shown that cell membrane penetrating particles can be used to cargo genetic materials in B16-F0 melanoma cells [27]. Finally, Lund et al. [28] have recently shown that via an energy-independent diffusion across the cell membrane, gold NPs coated with a 1:1 molar mixture of PEG-NH_2 and glucose ligands are taken up 18 times faster than NPs coated with either PEG-NH2 or glucose.

Our previous studies were based only on antigen-presenting dendritic mouse clonal DC2.4 cells [29] and mouse embryonic fibroblasts (MEFs) and did not compare the interaction of 'striped' particles with these two cell types. Also only limited time points were studied, and the core of the experiments was based on either 4 h [27], 3 h [20], or 1 h [20, 26] incubation times. To better establish the time evolution of NP uptake and to quantitatively compare between particle compositions and cell type, we have conducted here a set of systematic NP internalization experiments. We also introduce a generalized method to quantitatively measure the amount of NP-associated fluorescence localized in the cytosol of each cell by confocal laser scanning microscopy (CLSM).

We have chosen three different cell types for our investigation. First, we continued our work from previous investigations with DC2.4, which have a naturally high endocytotic activity [30]. In this study, we introduce 3T3 mouse fibroblasts and the human HeLa cervical cancer cell line. Care was taken to choose three unique cell lines that were known to exhibit differences in phenotype, cell division times, and endocytotic uptake [31–33].

2 Experimental

2.1 Experimental Materials

6-(((4,4-difluoro-5-(2-pyrrolyl)-4-bora-3a,4a-diaza-s-indacene3yl)styryloxy)acetyl) aminohexanoic acid, succinimidyl ester (BODIPY® 630/650-X, SE) was purchased from Invitrogen and thiolated through the succinimidyl ester group (BODIPY-SH) and MUS were synthesized in-house; both according to previously published methods [25]. All other chemicals were purchased from Sigma-Aldrich. All solvents were reagent grade and were purged with nitrogen gas for 60 min directly before use. All cell culture reagents were purchased from Invitrogen.

2.2 Synthesis of Fluorescently Labeled Gold NPs

0.9 mmol of gold salt ($HAuCl_4$) was dissolved in 150 mL purged ethanol, and the reaction vessel was subsequently kept under a light flow of nitrogen for the duration of the experiment. 0.9 mmol of the desired molar ratio of the thiol ligands (66-34OT, 34-66OT, 66-34br-OT, 100MUS) was dissolved in 10–20 mL of purged methanol and then added into the stirring reaction solution. A saturated sodium borohydride ($NaBH_4$) solution was prepared in 150 mL purged ethanol and added dropwise to the gold/thiol mixture. The solution was stirred for 3 h under nitrogen flow

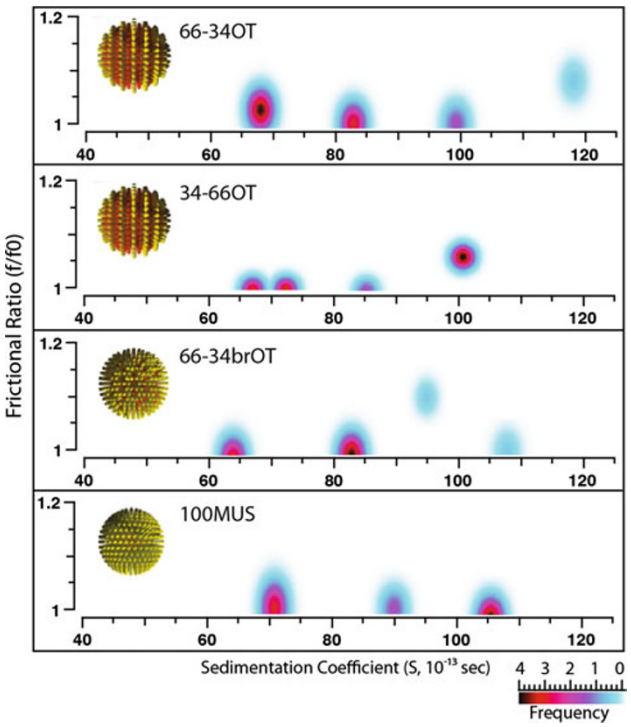

Fig. 1 Analytical ultracentrifugation size distributions. AUC sedimentation coefficient distributions for 66-34OT, 34-66OT, 66-34brOT, and 100MUS [34]. All four types of NPs show little difference in size. The axes of the plot are sedimentation coefficient (x) and frictional ratio (y). The former is a function of size and density; the latter is density dependent, thus a function of size and shape. The z axis displays the relative concentration of each peak

on ice and subsequently placed in a refrigerator overnight. The precipitated particles were collected via vacuum filtration with quantitative filter paper, washed with ethanol, methanol, and acetone and dried under vacuum. We further purified the NPs by centrifugal dialysis membranes (MW cutoff of 10,000 Da) in order to remove free ligands (as confirmed by 1H-NMR). The final NPs were characterized by TEM and AUC (Fig. 1). Further details of nanoparticle characterization can be found in the Supplementary Information.

A stock solution of BODIPY-SH dye in DI-H_2O/DMF (2:1 vol:vol) was used to place exchange $\sim$80-fold molar excess onto the NPs (dissolved in 750 μL of DI-H_2O) over 4 days. The reaction was purified of excess dye by centrifugation [20].

2.3 Cell Culture and NP-Cell Incubations

2.3.1 Maintenance

Each cell line was cultured in the appropriate medium with 10% fetal bovine serum (FBS) (Qualified FBS, US approved), 50 U mL^{-1} Penicillin and 50 U mL^{-1} Streptomycin at 37°C. The DC2.4 cells were cultured in RPMI medium, the HeLa tumor cells in DMEM medium with 1% Amphotericin B (Fungizone), and the 3T3 fibroblast cells in DMEM, High Glucose Glutamax with 10 mM HEPES. Each line was passaged with 0.05% Trypsin–EDTA every 3–4 days for regular maintenance.

2.3.2 Preparation of Nanoparticles

Dried NPs were dissolved in milli-Q purified water to a final concentration of 1 mg/mL. The solutions were shortly sonicated, passed through a 0.22 μm membrane filter to remove precipitates and immediately incubated with cells or stored at 4°C for future use. The final concentration of each particle solution was confirmed with UV–Vis spectrometry to have lost less than 5% NP mass after filtration (Supplementary Figure S1) or was assumed to be unchanged after filtration, if no residual NPs were visible in the filters. Concentrations were determined in solution by absorbance using a calibration curve previously prepared with dried NPs (Supplementary Figure S2).

2.3.3 Nanoparticle Incubations with Cells

Each cell line was plated in 8-well ibidi μ-slide chambers (ibidiTreat) at a starting concentration of 1.5–2.0 $\times$ 10^4 cells per well in 300 μL serum-containing medium. After 20–22 h, the medium was replaced in each well with 90 μL of fresh serum-containing medium. The final concentration for each NP incubation was 0.1 mg/mL; therefore 10 μL of each NP solution was added directly to the respective wells and mixed thoroughly. 10 μL of milli-Q purified water was added to the control well. For the 4°C measurements, all reagents and cells were pre-cooled for 30 min prior to NP addition. After the appropriate length of incubation time, the NP solutions were removed from the wells, and each well was washed three times with 200 μL of serum-containing medium. The cells were left in the last wash and immediately imaged. The short-term live-incubated NP-internalization imaging was performed directly on unwashed samples at 37°C.

2.4 Fluorescence Confocal Microscopy and Data Analysis

All imaging was performed with live cells on a Zeiss LSM 700 Inverted Microscope. Transmission and confocal laser scanning images were recorded with a 63×/1.40 oil objective lens at an excitation wavelength of 630 nm and an emission wavelength of 650 nm using a solid state HeNe laser. All images were collected at identical laser settings. Care was taken to select planes, or slices, during imaging that were clearly located inside of the cells, by first passing the cells in the z axis on both sides, and returning to an internal slice.

The direct short-term time-lapse imaging experiments during NP incubation were performed using the Zeiss LSM 700 with an additional Okolab CO_2 Microscope Stage incubator CRYO WJ to maintain an environment of 37°C and 5% CO_2. The analysis of all confocal data was performed with MetaMorph 7.7 (2011 Molecular Devices). A plug-in was created that allowed the manual tracing of representative areas of background, cell membranes, and nuclei for each confocal image, performed on the overlapped transmission and red fluorescent channels. The regions of interest were used to quantify the intracellular fluorescence in the cytoplasm only. For each cell, the integrated fluorescence intensity of the nucleus was subtracted from the total integrated intracellular fluorescence intensity, and divided by the total cell area minus the nuclear area, in order to obtain the average fluorescence intensity per unit area in the cytosol. Two independent average fluorescent intensities for small regions of interest in the background of each image were averaged and subtracted from the average cytosolic intensity to obtain the final, background-corrected, nucleus-subtracted average cytosolic fluorescence intensity. This process is illustrated for a typical confocal image in Fig. 2. About 10–30 cells were analyzed for each NP-cell incubation and their fluorescence averages and standard deviation plotted in Fig. 3.

3 Results and Discussion

Four types of monolayer-protected gold NPs were synthesized and incubated with three different cell lines. The particles tested were (1) 100MUS: homoligand 11-mercapto-1-undecanesulphonate (MUS), (2) 66-34OT: a 2:1 molar mixture of MUS and 1-octanethiol (OT), (3) 34-66OT: a 1:2 molar mixture of MUS and OT and (4) 66-34br-OT: a 2:1 molar mixture MUS and 3,7 dimethyl octane 1-thiol (br-OT). As with previous investigations [20] we confirmed that the size distributions of the four types of NPs had negligible differences and that the particles were free of unbound ligands. The composition and structure of the ligand shell were the only physical characteristics varied between the particles. Figure 1 illustrates that the size distributions of the NPs showed negligible differences by analytical ultracentrifugation [34]. Since the sedimentation coefficient is dependent chiefly on the size and shape of the NP (the latter being constant for spherical NPs, as exhibited by the frictional ratio plotted on the *y* axis), we can affirm that the size range between NP types is very similar. Therefore we assume that any effects arising from differences in size between NP types are absent. The composition of the particles mentioned above is the stoichiometric one used in the synthesis reaction. The actual composition scales with the synthetic one, [25] but is difficult to determine precisely. We have done NMR investigations (see Supplementary Information) after particle decomposition to confirm the proportionality between the stoichiometric ratio and the final ligand shell composition.

To study the uptake and subsequent distribution of the NPs in the cell, we labeled each particle with thiolated BODIPY-SH dye, chosen due to its minimal overlap in emission spectra with normal cellular fluorescence and NP absorption, and its high quantum yields [35]. We first confirmed that the magnitude of fluorescence was independent of surface composition or structure, i.e., each type of NP was functionalized with an identical amount of BODIPY-SH dye. We prepared a sample of each type of NP at the same absorbance at 520 nm by UV–Vis spectroscopy and confirmed that the magnitude of fluorescence was equal between them. After particle decomposition (see Supplementary Information), we calculate that less than 10% of the total ligands presented on the NP surface are place-exchanged by dye molecules, and therefore assume that their presence does not significantly affect the surface structure. We have also previously shown that the presence of the fluorophore does not affect the penetration properties of our NPs, by comparing penetration results with and without fluorophores determined via TEM [20] or photothermal heterodyne imaging [26], techniques that do not necessitate the use of fluorophores for quantification.

Each of the four types of NPs was incubated in three different cell lines: DC2.4 dendritic cells, HeLa cancer cells, and 3T3 fibroblasts. Several incubation times of NPs with cells were chosen: 1, 3, 8, 24, 48, and 72 h at two temperatures, 37 and 4°C. As the cells were visibly unstable after 24 h at 4°C, the 48 and 72 h time points were excluded. Representative CLSM images from incubations for 8 h at 37°C and 3 h at 4°C are presented in Fig. 4. The results indicate that the 66-34OT NPs internalize the most into the cytoplasm of each cell line under both conditions. At 37°C, the 66-34OT particles exhibit a bright, diffuse pattern of intracellular fluorescence in addition to punctuate fluorescence indicative of endosomal uptake, whereas the other particles display primarily punctuate fluorescence. At 4°C, where energy-mediated endocytotic processes are inhibited, the 66-34OT NPs permeate the most into each cell line. This result supports our conclusion that the 66-34OT NPs are capable of bypassing the endocytotic pathways and directly penetrating into the cell.

We have plotted the cytoplasmic average fluorescence intensities (background and nucleus corrected) of the CLSM images for each cell type and NP at all the aforementioned incubation times and temperatures in Fig. 3. For all analyzed conditions at 37°C, the 66-34OT NPs exhibit higher cytosolic internalization. The 34-66OT and

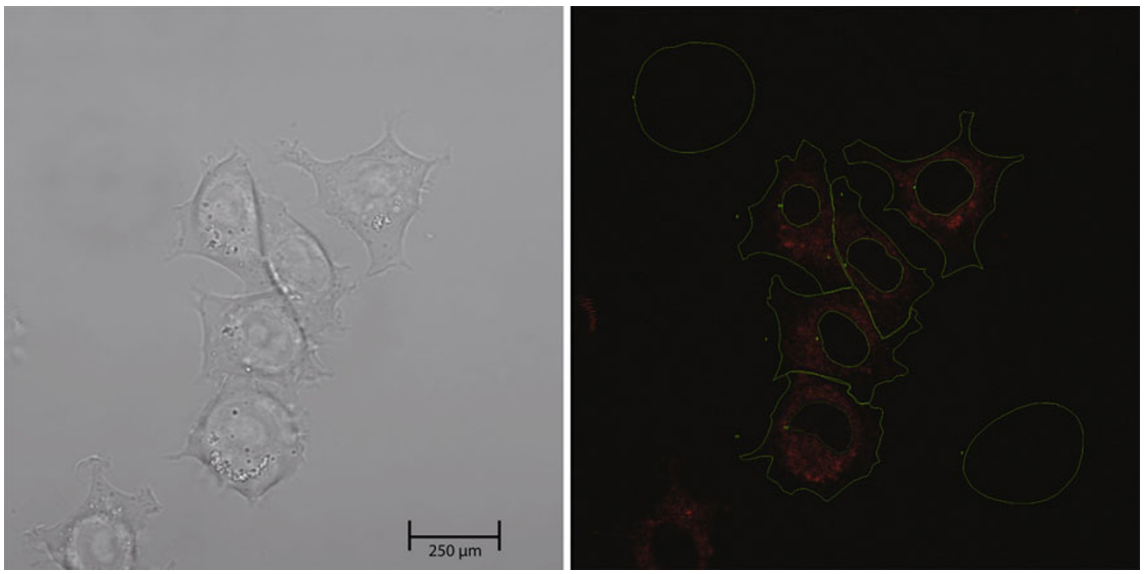

Fig. 2 Methodology for fluorescence quantification of CLSM images. Regions of interest (ROIs; *green outlines*) were hand-drawn on overlapped transmission *(left)* and *red channel* images *(right)* for each treatment. ROIs were drawn around the cell membrane, nucleus and the background of each image. Final fluorescence intensities were calculated from the *red channel* only (*right*). The final cytoplasmic fluorescence intensities were calculated as described in Sect. 2

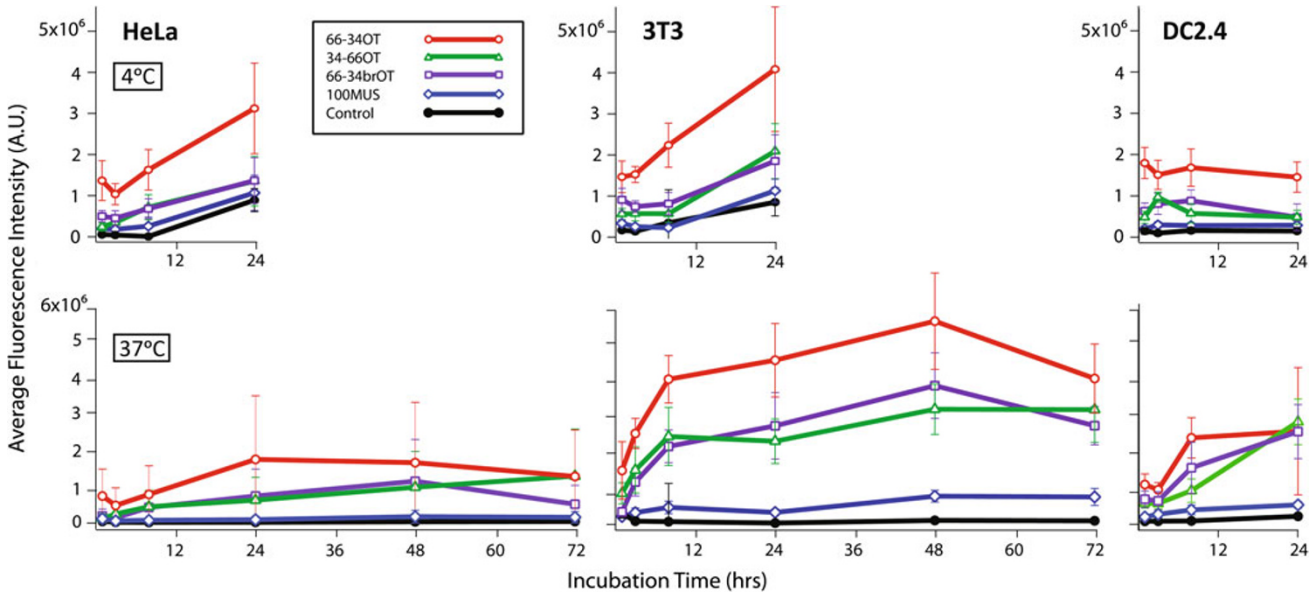

Fig. 3 Cytoplasmic fluorescence quantification of np internalization. Average cytoplasmic fluorescence intensities of HeLa, 3T3, and DC2.4 incubated with 100MUS, 66-34br-OT, 34-66OT, and 66-34OT NPs for 1, 3, 8, 24, 48, and 72 h at 4°C (*top*) and 37°C (*bottom*). Error bars represent one standard deviation of the mean

66-34br-OT fluorescence intensities are similar to each other, within each cell type and the 100MUS was internalized the least. The DC2.4 cells remained visibly healthy only up to 24 h, therefore the 48 and 72 h time point were excluded. In the case of DC2.4 cells, all of the particles except for 100MUS were internalized approximately to the same extent after 24 h at 37°C. This result could be attributed to the loss of a self-regulation endocytotic mechanism in this cell line. Between each cell line, the 3T3 cells exhibited the highest fluorescence intensity at each time point. This result suggests that the membrane composition of the 3T3 cells is more permeable to the particles [33].

At 4°C, we found similar trends for each cell line, with the 66-34OT NPs internalized the most at each time point. After 8–24 h, the cells were visibly unhealthy due to the cold conditions, yet the 66-34OT particles still selectively

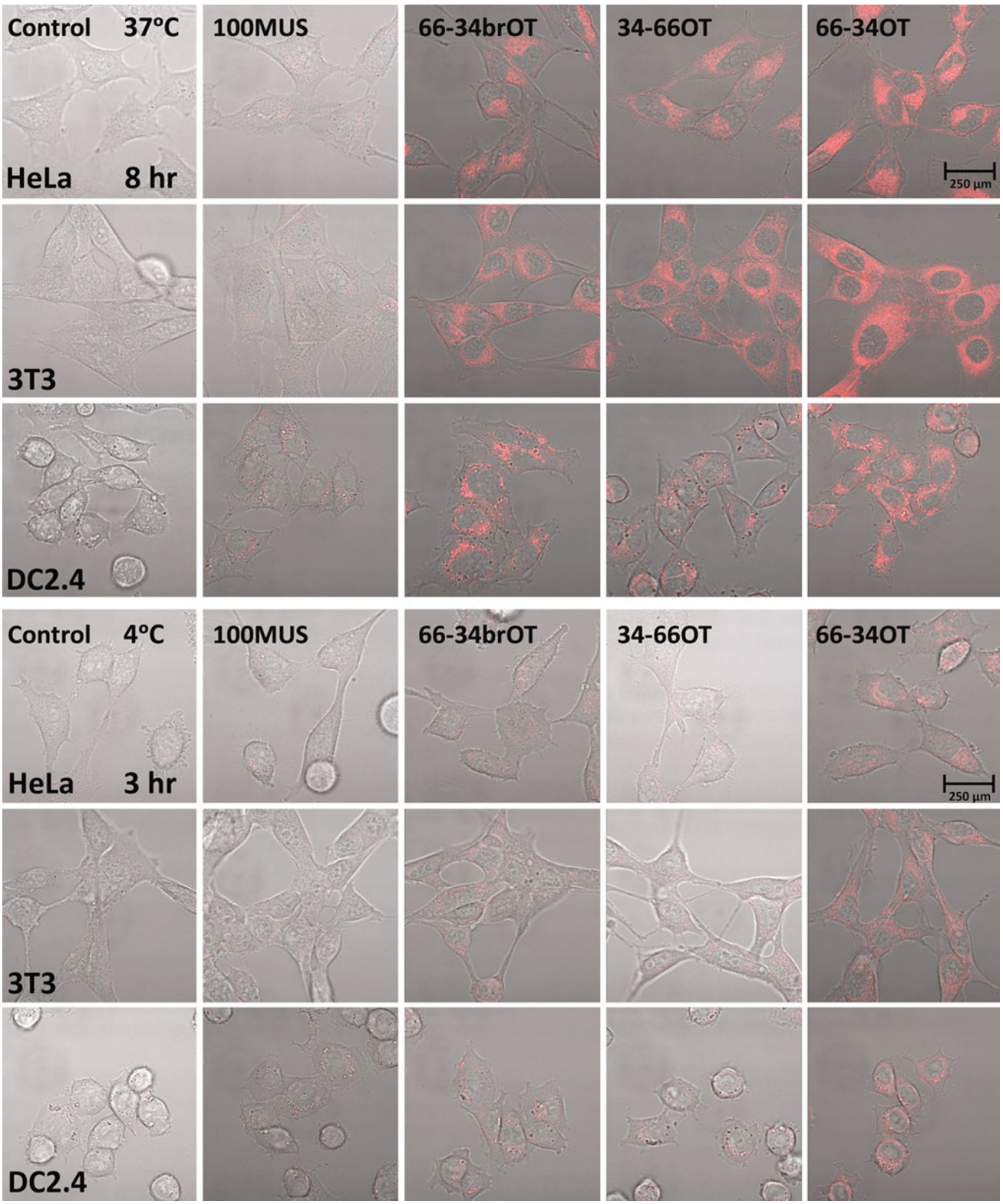

Fig. 4 Confocal microscopy images of NP-cell internalization. Representative images of live HeLa, 3T3, and DC2.4 cells incubated with 100MUS, 66-34br-OT, 34-66OT, and 66-34OT NPs. The *top panel* displays incubations for 8 h at 37°C while the *bottom panel* shows incubations for 3 h at 4°C. Cells were washed three times before imaging. Each image was captured with identical laser power, gain, and intensity settings on the CLSM

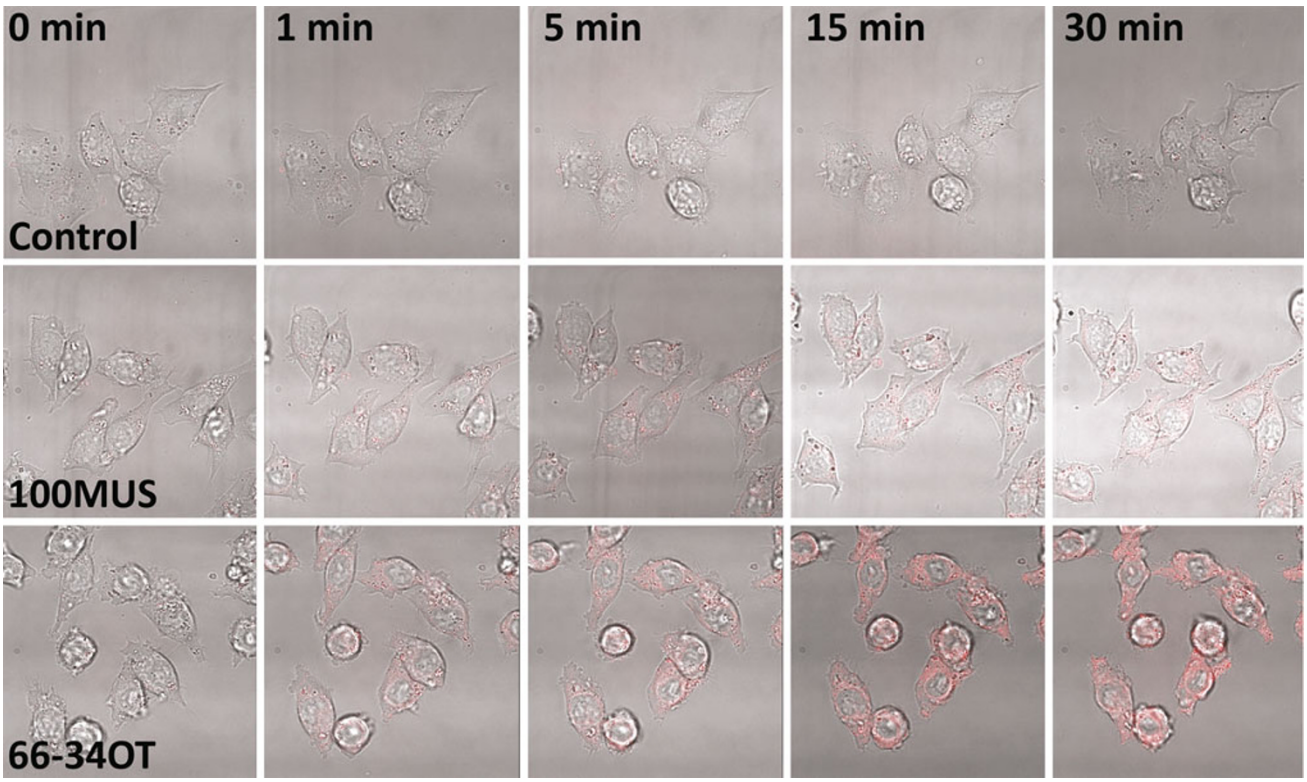

Fig. 5 Short-term live-incubation NP-cell internalization. DC2.4 cells were imaged immediately following direct incubation with 100MUS or 66-34OT NPs at 1, 5, 15, and 30 min in order to capture internalization behavior at short times. The 0 min images were captured before NP addition

permeated into the cytoplasm higher than any other NP at these later time points.

The short-term NP incubation was imaged live with 100MUS and 66-34OT NPs added to DC2.4 cells directly at the CLSM. The results in Fig. 5 show that the 66-34OT NPs begin to penetrate the lipid bilayer within 1 min at 37°C. The diffuse pattern of fluorescence within shorter time frames further supports the capability of the 66-34OT NPs to directly penetrate the cell membrane, as endocytotic and pinocytotic pathways take place on a longer time scale [36].

An interesting result of our study is that most of the variation in fluorescence intensity occurs in the earlier time points, up to just a few hours after NP incubation. To illustrate this argument, we have plotted the rate of change in fluorescence intensity against the incubation time for all cell lines, time points, and temperatures (Fig. 6). The plots quickly dampen to nearly no significant changes among cell lines and/or NP type after 8 h. This trend is invariant with respect to NP and cell type, indicating that there is a fundamental biological effect occurring in our system. It has been shown that size may play a crucial role in the long-term penetration. A similar study with smaller surface-structured NPs ($\sim$2 nm core size) showed that uptake rates did not decrease at long times [28]. Previously, it has been shown that competing thiolated molecules presented by the cell in high molar quantities can completely replace the original ligand shell of the trafficked NPs, and that this process occurs in a characteristic time period of several hours to days [37]. It is also well known that this destabilization can lead to NP aggregation, so that the NP diffusion and cell internalization behavior would be significantly altered [37, 38]. Therefore we can conclude that the surface structure initially presented on the NPs has little to no effect on cell internalization at time points past a few hours for larger gold NPs. To better understand the temporal progression between structure-dominated penetration and a more classical endocytosis-dominated penetration, future work will include a time-resolved analysis of the ratio between punctuate and diffuse fluorescence.

Future work will also need to explore several questions raised by this investigation. First, we will confirm the results of our study by flow cytometry. In addition, the techniques optimized in this study will be used to compare the internalization behavior of an even larger variety of cell types, compositions of MUS:OT and MUS:brOT, and a changing length of the sulfonate-capped ligand. We will also use these techniques to quantify how the role of NP size, both of the core and ligand shell, affects cell uptake.

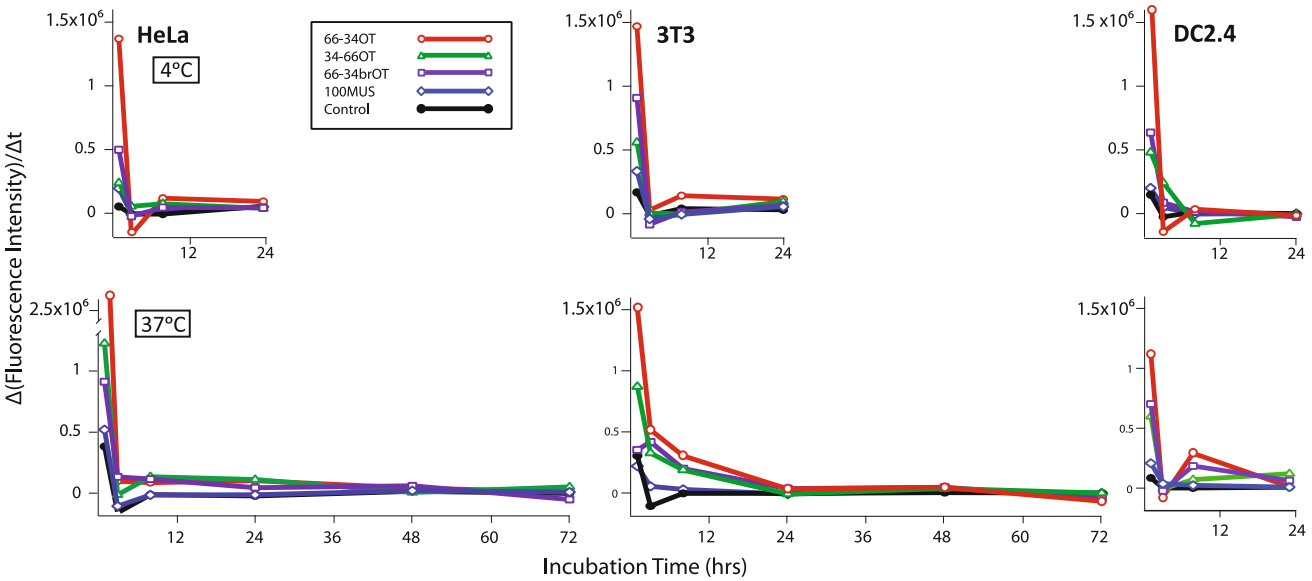

Fig. 6 Rate of change of fluorescence intensity versus incubation time for HeLa, 3T3, and DC2.4 cells at both 4 and 37°C. It is apparent that most of the variation in fluorescence intensity (and therefore NP internalization) is found in early times under a few hours

In addition, we will test the role of the hydrophobic ligand, to determine the extent that it affects internalization.

4 Conclusion

The present study outlines a NP-cell-interaction procedure that can be used to characterize cellular internalization by quantitative CLSM. In three distinct cell lines, DC2.4 dendritic mouse clonal cells, 3T3 mouse fibroblasts, and the human HeLa cervical cancer cells, we observed a time- and temperature-dependent internalization behavior with respect to several types of mixed monolayer-protected NPs differing in ligand structure and composition. Homoligand 100MUS were internalized consistently lower than any type of mixed-ligand NP. Between three types of mixed-ligand NPs, the unstructured 66-34br-OT was indistinguishable from the surface-structured, predominantly hydrophobic 34-66OT. The highest amount of cellular internalization for all cell types, temperatures, and incubation times was found with the surface-structured, hydrophilic 66-34OT NPs. We also show that these NPs are internalized into cells at very short time scales of under 1 min. This methodology can be used to screen between a variety of surface compositions and structures of monolayer-protected NPs in order to study NP-cell internalization behavior.

Acknowledgments The authors would like to thank Prof. Heinrich Hofmann for support and equipment. They also acknowledge Floyd Sarria Juan-Carlos at the BioImaging and Optics Platform of EPFL for writing the MetaMorph plug-in for image quantification analysis. This work was supported by the Swiss National Foundation NRP 64 program.

References

1. Han G, Ghosh P, Rotello VM (2007) Nanomedicine (Lond) 2(1):113
2. Kievit FM, Zhang M (2011) Adv Mater 23(36):H209
3. Chanana M, Correa-Duarte MA, Liz-Marzan LM (2011) Small 7(18):2650
4. Otsuka H, Nagasaki Y, Kataoka K (2003) Adv Drug Deliv Rev 55(3):403
5. Ferrari M (2005) Nat Rev Cancer 5(3):161
6. Willets KA, Van Duyne RP (2007) Annu Rev Phys Chem 58:267
7. Xue XJ, Wang F, Liu XG (2011) J Mater Chem 21(35):13107
8. Kumari A, Yadav SK (2011) Expert Opin Drug Deliv 8(2):141
9. Templeton AC, Wuelfing WP, Murray RW (2000) Acc Chem Res 33(1):27
10. Centrone A, Penzo E, Sharma M et al (2008) Proc Natl Acad Sci USA 105(29):9886
11. Warner MG, Hutchison JE (2003) Nat Mater 2(4):272
12. Dhar S, Daniel WL, Giljohann DA et al (2010) J Am Chem Soc 132(48):17335
13. Mulder WJ, Strijkers GJ, van Tilborg GA et al (2009) Acc Chem Res 42(7):904
14. Wadia JS, Dowdy SF (2005) Adv Drug Deliv Rev 57(4):579
15. Pagliara A, Reist M, Geinoz S et al (1999) J Pharm Pharmacol 51(12):1339
16. Yu J, Patel SA, Dickson RM (2007) Angew Chem Int Ed Engl 46(12):2028
17. Dobson PD, Kell DB (2008) Nat Rev Drug Discov 7(3):205
18. Allen TM, Cullis PR (2004) Science 303(5665):1818
19. Shukla R, Bansal V, Chaudhary M et al (2005) Langmuir 21(23):10644
20. Verma A, Uzun O, Hu Y et al (2008) Nat Mater 7(7):588
21. Jackson AM, Myerson JW, Stellacci F (2004) Nat Mater 3(5):330

22. Devries GA, Brunnbauer M, Hu Y et al (2007) Science 315(5810):358
23. Glotzer SC, Anderson JA (2010) Nat Mater 9(11):885
24. Glotzer SC (2004) Science 306(5695):419
25. Uzun O, Hu Y, Verma A et al (2008) Chem Commun (Camb) (2):196
26. Leduc C, Jung JM, Carney RR et al (2011) ACS Nano 5(4):2587
27. Jewell CM, Jung J, Atukorale PU et al (2011) Angew Chem Int Ed 50:1
28. Lund T, Callaghan MF, Williams P et al (2011) Biomaterials 32(36):9776
29. Hu Y, Litwin T, Nagaraja AR et al (2007) Nano Lett 7(10):3056
30. Banchereau J, Steinman RM (1998) Nature 392(6673):245
31. Wu H, Gao SB, Sakurai T et al (2011) Chin J Integr Med
32. Shan Y, Ma S, Nie L et al (2011) Chem Commun (Camb) 47(28):8091
33. Xu H, Dai W, Han Y et al (2010) J Nanosci Nanotechnol 10(11):7406
34. Carney RP, Kim JY, Qian H et al (2011) Nat Commun 2:335
35. Loudet A, Burgess K (2007) Chem Rev 107(11):4891
36. Wiley HS, Cunningham DD (1982) J Biol Chem 257(8):4222
37. Stark WJ (2011) Angew Chem Int Edit 50(6):1242
38. Limbach LK, Li YC, Grass RN et al (2005) Environ Sci Technol 39(23):9370